Three-dimensional Reconstruction of an Actin Bundle

Esther S. A. Bullitt,* David J. DeRosier,‡ Lynne M. Coluccio,§ and Lewis G. Tilney§

*Graduate Program in Biophysics, ‡Rosenstiel Basic Medical Sciences Research Center, Brandeis University, Waltham, Massachusetts 02254; and §Department of Biology, University of Pennsylvania, Philadelphia, Pennsylvania 19104

Abstract. We present the three-dimensional structure of an actin filament bundle from the sperm of *Limulus*. The bundle is a motile structure which by changing its twist, converts from a coiled to an extended form. The bundle is composed of actin plus two auxiliary proteins of molecular masses 50 and 60 kD. Fraying the bundle with potassium thiocyanate created three classes of filaments: actin, actin plus the 60-kD protein, and actin plus both the auxiliary proteins. We examined these filaments by transmission electron microscopy and scanning transmission electron microscopy (STEM). Three-dimensional reconstructions from electron micrographs allowed us to visualize the actin subunit and the 60- and 50-kD subunits bound to it. The actin subunit appears to be bilobed with dimensions 70 × 40 × 35 Å. The inner lobe of the actin subunit, located at 20 Å radius, is a prolate ellipsoid, 50 × 25 Å; the outer actin lobe, at 30 Å radius, is a 35-Å-diam spheroid. Attached to the inner lobe of actin is the 60-kD protein, an oblate spheroid, 55 × 40 Å, at 50 Å radius. The armlike 50-kD protein, at 55 Å radius, links the 60-kD protein on one of actin's twin strands to the outer lobe of the actin subunit on the opposite strand. We speculate that the 60-kD protein may be a bundling protein and that the 50-kD protein may be responsible for the change in twist of the filaments which causes extension of the bundle.

ACTIN, a protein found in essentially all eukaryotic cells, is used by cells for both motility and cytoskeletal support. The structure of actin and how it combines with auxiliary proteins define the role actin performs in a particular structure. One such motile structure is found in the sperm of *Limulus*. It is a bundle of actin filaments cross-linked by auxiliary proteins. Initially the bundle is coiled to form a compact structure at the posterior end of the sperm cell. During fertilization of the egg, the bundle uncoils to generate a 60-μm-long acrosomal process (Tilney, 1975). The uncoiling is driven by a change in twist of the actin-containing filament (DeRosier et al., 1980). The entirely different functions and movements which actin filaments perform seem to arise from the particular set of actin binding proteins associated with each actin-containing structure (compare the role of actin in the extension of the *Limulus* acrosomal process, for example, to interactions between actin and myosin in contracting skeletal muscle or cytokinesis). To understand better how actin can perform different functions in different structures, we need to determine the three-dimensional structure of F actin as well as actin in combination with its auxiliary proteins. Actin filaments, however, are disordered, making analysis difficult (Aebi et al., 1986; Egelman and DeRosier, 1983).

Here we report studies of actin-containing filaments which we show have little angular disorder, presumably due to the presence of auxiliary proteins. Our analysis of these ordered filaments allows us to avoid the difficulties inherent in studying disordered systems. We obtained three classes of filaments, denoted 5.9, 4.0, and 1.6. The last is pure actin. Negatively stained preparations of the two other classes of filaments showed little, if any, of the disorder seen in filaments of pure F-actin. The high degree of helical order made these filaments well-suited for three-dimensional (3D)[1] reconstruction. SDS-PAGE, mass determination with the scanning transmission electron microscope (STEM) at Brookhaven National Laboratory (Brookhaven, NY) and 3D reconstruction techniques demonstrated that the 4.0 filaments are composed of F-actin complexed with an equimolar amount of a 60-kD protein while the 5.9 filaments contain actin with equimolar amounts of both the 60- and 50-kD proteins. These filaments were used to determine the structure of actin, the 60-kD protein, and the 50-kD protein, as well as to show how these two auxiliary proteins bind to actin and how the filaments interact to form a bundle.

Materials and Methods

Specimen Preparation

Bundles in the false discharge state were isolated from *Limulus* (horseshoe crab) sperm as described by Tilney (1975). The isolated false discharges

L. M. Coluccio's present address is Cornell University, Ithaca, NY 14850.

1. *Abbreviations used in this paper*: KSCN, potassium thiocyanate; STEM, scanning transmission electron microscopy; 3D, three dimensional.

were frayed by treatment with 0.5 M potassium thiocyanate (KSCN) or 0.8 M potassium iodide (KI) for 0–15 min. The fraying reaction was stopped by dilution with 10 mM Tris-HCl, and the extent of the reaction was checked by electron microscopy. In some cases the isolated bundles were allowed to sit on ice for a few days (2–7 d) during which fraying occurred without the need for KSCN or KI. As a control F actin filaments were prepared as described by Spudich and Watt (1971), and then treated with 1% Triton X-100 and 0.5 M KSCN.

SDS Gel Electrophoresis

The isolated, intact acrosomal bundles were analyzed by discontinuous SDS-PAGE with a 5% stacking gel and a 12% resolving gel (Laemmli, 1970). Bio-Rad Laboratories (Richmond, CA) low molecular mass standards (14.4–92.5 kD) were used to determine approximate molecular masses.

Transmission Electron Microscopy

The treated false discharge sample was placed on a carbon-coated electron microscope grid, washed with 10 mM Tris-HCl pH 7.5 or 10 mM sodium phosphate pH 6.7, and negatively stained with 1 or 2% uranyl acetate. Electron photomicrographs were taken on a Philips EM200, a Philips EM301, or a Philips EM420 at 60, 80, or 100 kV, respectively.

STEM

Measurements of mass-per-unit length were performed on the STEM at Brookhaven National Laboratory using the method of Wall and Hainfeld (1986). A drop of 5 mM sodium phosphate (pH 7) was placed on a wet carbon-coated (20-Å-thick film) titanium electron microscope grid. The treated false discharge sample or similarly treated F-actin sample was injected into the drop and adsorbed to the carbon film for 1 min. The grids were washed with 5 mM sodium phosphate, frozen in nitrogen slush, and freeze-dried for 12 h. Grids were transferred to the cold stage without exposure to the atmosphere via a transfer unit. The values for the mass-per-unit length and radial density profiles were determined as in Steven et al. (1986, 1984), using tobacco mosaic virus particles as a standard. We measured mass per unit length for segments of filaments ~500–1,500 Å long, and measured the radial density profile for straight segments of filaments 500–1,000 Å long. Data for the profiles were taken from 16 of the 5.9 filaments, 19 of the 4.0 filaments, and 31 of the actin (or 1.6) filaments. The radial density plots were scaled and subtracted to produce radial density profiles of the 50-kD protein (the 5.9 profile minus the 4.0 profile) and the 60-kD protein (4.0 minus 1.6).

Computer Analysis

Electron microscope negatives were digitized using an Optronics P-1000 densitometer with a spot size of 50 μm and 256 grey levels, yielding a maximum resolution of ~30 Å. Images were floated on a background value which is the average of the perimeter values. The Fourier transforms and three-dimensional helical reconstructions were computed as described by DeRosier and Moore (1970), but with an array of 512 by 512 points. Extraction of amplitudes and phases along the layer line was done by interpolation of data in Fourier space where the data were oversampled; interpolation of data on the image was not done since that caused a loss of power in the higher resolution data. The computations were done on a Digital Equipment Corporation VAX 11/780 computer and displayed on the Grinnell GMR-27 or AED-512 graphics systems. The basic computer programs for the helical reconstruction were those developed at the Medical Research Council Laboratory of Molecular Biology (Cambridge, England) and adapted to our VAX.

Calculating Cumulative Angular Disorder

To calculate the angular disorder, we determined $\Delta\phi_{obs}$, the angle of rotation per subunit in the helix. $\Delta\phi_{obs} = 360°/(2 + a/b)$, where a and b are the axial heights of the first (1/355 Å) and sixth (1/59 Å) layer lines, respectively (DeRosier and Censullo, 1981). The uncertainty, d_i, of $\Delta\phi_{obs}$ for a particular filament increases as $\sqrt{N}$, where N is the number of subunits in the i^{th} filament:

$$d_i = \sqrt{N}(\Delta\phi_{obs} - \Delta\phi_{avg}), \quad (1)$$

where $\Delta\phi_{avg}$ is the overall average of $\Delta\phi_{obs}$ for all filaments measured (Egelman and DeRosier, 1982). The angular disorder of all filaments measured is then the root mean square (*rms*) value of d_i, that is:

$$d_{rms} = \sqrt{\frac{\sum d_i^2}{n-1}}, \quad (2)$$

where n is the number of filaments used for the calculation.

Calculation of Q and Phase Residuals

We examined layer lines l = 0, 1, 2, 5, 6, 7 (equator, 1/355, 1/177, 1/71, 1/59, 1/51 Å) with regard to their intensity and radial resolution, and the symmetry of the phases about the meridian.

One criterion for choosing a filament for inclusion in the reconstruction was the minimum value of Q, where $Q = (\Sigma|F||\Delta\theta|)/(\Sigma|F|)$ with $|F|$'s the amplitudes and $\Delta\theta$'s the phases of the layer line data (DeRosier and Moore, 1970). Minimization of Q corresponds to the displacement of the phase origin and the tilt angle of the filament out of the plane of the projection which yields data most consistent with helical symmetry. Lower values for Q correspond to filaments that more nearly possess strict helical symmetry. A second measure of the quality of the data was found in scaling data sets from different images prior to averaging. The images were aligned and scaled by minimizing the amplitude-weighted phase residual (Amos, 1975):

$$R(\Delta\phi, \Delta z) = \sqrt{\frac{\Sigma|F||\Delta\theta|^2}{\Sigma|F|}}, \quad (3)$$

where $\Delta\theta = \phi_1 - \phi_2 - n\Delta\phi + 2\pi\Delta zZ$. The lower the minimum value of R, the better the agreement between data sets.

Real-Space Residuals

The 4.0 class filament reconstruction was aligned to the 5.9 class filament reconstruction by minimization of a real-space residual as follows:

$$\text{R.-S. Residual} = \sum_i(\rho_{i,4.0})^2 - \sum_i \rho_{i,4.0}\rho_{i,5.9}, \quad (4)$$

where ρ_i is the density value at the i^{th} pixel in the asymmetric unit. This somewhat unusual form of a residual attempts to fit the actin + 60-kD protein portion of the two filaments. The more usual form, $\Sigma(\rho_{i,4.0} - \rho_{i,5.9})^2 = \Sigma(\rho_{i,4.0})^2 - 2\Sigma\rho_{i,4.0}\rho_{i,5.9} + \Sigma(\rho_{i,5.9})^2$, will have a constant "background" which prevents the minimum from being zero. This background arises in the term $\Sigma(\rho_{i,5.9})^2$ from those features that are not part of the 4.0 filament (that is, from the 50-kD protein). The change in the equation does not shift the position of the minimum, but merely modifies its depth.

Results

Composition of the Intact Bundle

We determined the composition of the *Limulus* acrosomal process using SDS-PAGE. As judged by light microscopy, preparations of the bundles primarily contained false discharges, with a small percentage of true discharges. Gels of these preparations showed proteins of apparent molecular masses 97, 59, 53, and 43 kD (Fig. 1). This is in contrast to the apparent molecular masses of 95, 55, and 43 kD reported earlier by Tilney (1975) who used a tube-gel system without a stacking gel. Using a discontinuous gel system (Laemmli, 1970), we resolved the "55 kD" into two proteins whose apparent molecular masses were 59 and 53 kD; STEM measurements (next section) indicate the presence of subunits having masses of 63 kD and 49 kD, respectively. We think the two bands correspond to the two subunits (see Discussion). For simplicity of nomenclature we call the two auxiliary proteins 60 kD and 50 kD. P. Matsudaira (personal communication) prepared samples of isolated false discharges free of true discharges, and samples of true discharges free of false discharges. Both had the 43-kD actin band. He found, however, a 110-kD protein (presumably the same as our 97-kD band) only in preparations of isolated true discharges, and the pair of bands around 55 kD only in

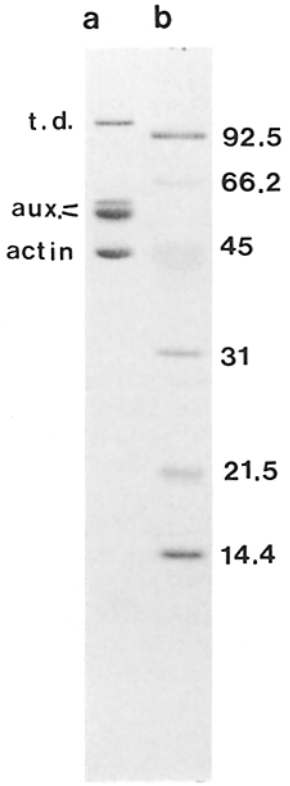

Figure 1. SDS-PAGE of actin bundles from the sperm of *Limulus*. (*a*) The bundle preparation after its isolation but before any fraying with a chaotropic agent. The band corresponding to actin is marked. The two bands with apparent molecular masses of ~50 and 60 kD are marked "aux". The band at 100 kD (*t.d.*) is a contaminant from the true discharge form of the bundle. (*b*) Molecular mass standards.

preparations of false discharges. This 110-kD band may correspond to a cross-linked dimer of the 50 and 60 kD proteins. The 97-kD component found in our preparations is most likely due to the presence of contaminating true discharges and, therefore, the false discharge is composed of actin (43 kD) plus two auxiliary proteins (60 and 50 kD).

Composition of Single Filaments

The isolated false discharges were treated with KSCN, which induces bundles to fray into individual filaments (Fig. 2). The KSCN-treated preparations contain more than one class of helical filaments. There are filaments ~150 Å in diameter (Fig. 2, *arrow*), and filaments ~100 Å in diameter (Fig. 2, *arrowhead*). What is needed is to separate the frayed filaments into classes and to determine the composition of each. SDS-PAGE analysis is not useful here, as we have been unable to isolate one type of filament free of the others. Instead, we examined individual filaments using the mass per unit length capabilities of the STEM at Brookhaven National Laboratory. This solved the problem of heterogeneity in a population of filaments frayed from a bundle because we examined individual filaments. Furthermore, the accuracy of mass measurement of this technique is at least comparable to that of SDS-PAGE (see Wall and Hainfeld, 1986).

Figure 2. Electron micrograph of a negatively stained, frayed actin bundle. The intact bundle was frayed by brief treatment with KSCN. Two classes of filaments can be seen: one having a diameter of 150 Å, (*arrow*) and the other a diameter of 100 Å, (*arrowhead*). These were subsequently identified as a 4.0 filament and F-actin or 1.6 filament, respectively (see text). Bar, 2,500 Å.

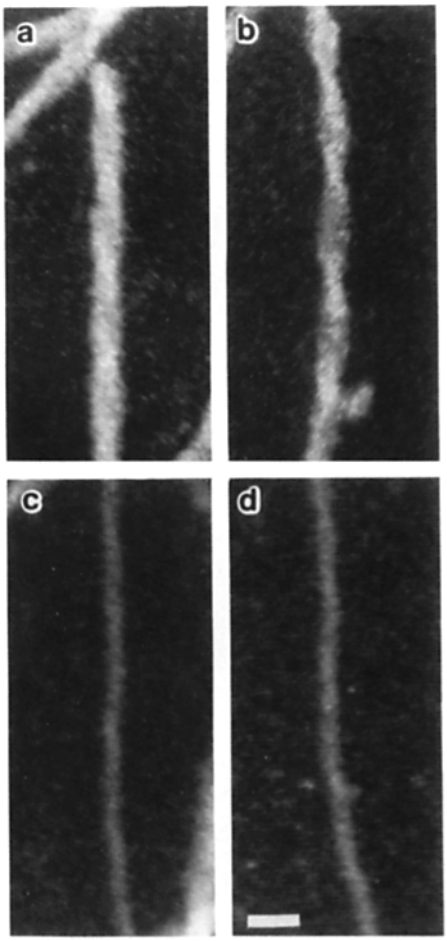

Figure 3. Scanning transmission electron micrographs of a freeze-dried, frayed actin bundle. (*a*) Filament with mass/length of 5.9 kD/Å. (*b*) Filament with mass/length of 4.0 kD/Å. (*c*) Filament with mass/length of 1.6 kD/Å. (*d*) Actin filament treated with KSCN. Bar, 200 Å.

When we examined the kinds of filaments found in frayed bundles we found three classes of filaments (Fig. 3, *a–c*) with the following mass per unit length: 1.6, 4.0, and 5.9 kD/Å (Fig. 4). We use these values to name the three classes. The composition of these classes of filaments can be deduced by converting their mass per unit length into mass per asymmetric unit by multiplying by the rise per asymmetric unit. To obtain the rise per asymmetric unit we measured the lengths of crossovers of the helix, known to contain 14 asymmetric units (DeRosier et al., 1977). The calculated symmetry yields a rise per subunit of 26.4 Å. Thus, a mass/length of 1.6, 4.0, or 5.9 kD/Å correspond to 43, 106, or 156 kD, respectively.

As a control we measured the mass per unit length of F-actin isolated and repolymerized from skeletal muscle. It was treated with KSCN and Triton X-100 before freeze-drying and examination with the STEM (Fig. 3 *d*). It has a mass per unit length of 1.6 kD/Å (Fig. 4 *d*). This provides an excellent control for the frayed *Limulus* filaments; the 1.6-filament is obviously pure actin, as it has an asymmetric unit of 43 kD, the expected mass of actin.

Given, by SDS-PAGE, that the *Limulus* false discharge consists of actin, a 60- and a 50-kD protein, the simplest interpretation of the three filament types is the following: the 1.6 filament is pure actin whose subunit mass is 43 kD. The 4.0-filament which gives an asymmetric weight of 106 kD corresponds to an equimolar combination of actin (43 kD) and the 60-kD protein. The 5.9 filament gives an asymmetric unit mass of 156 kD which corresponds to actin in equimolar combination with both the 60- and the 50-kD subunits. Three-dimensional reconstructions of these filaments (see below) support these assignments.

Distinguishing Filament Types

The results of the STEM measurements on freeze-dried preparations revealed three classes of filaments. The narrowest of these, having a diameter of ~100 Å (Fig. 3 *c*), is actin. The other two (5.9 and 4.0) have about the same diameter, 150 Å. In order to proceed with structural analysis we needed to distinguish between images of these two kinds of filaments in negatively stained preparations. In the images of the freeze-dried preparations, the 4.0 filaments were modulated strongly from crossover to crossover, being much narrower at the crossover than halfway between (Fig. 3 *b*). In contrast, the 5.9 filaments (Fig. 3 *a*) were only slightly modulated, having about the same outer diameter as the 4.0 filaments but a wider crossover. The differences in modulation were also seen in images of negatively stained preparations (Fig. 5, *a* and *c*), allowing us to distinguish between the two classes of filaments.

Analysis of Cumulative Angular Disorder

To carry out a three-dimensional reconstruction from images of single frayed filaments, we first needed to assess the angular disorder in filaments frayed from the *Limulus* bundle. 45 frayed *Limulus* filaments (12 of the 5.9 class and 33 of the 4.0 class of filaments) were chosen for analysis based on the straightness of the filament and on the presence of at least the first and sixth layer lines (Fig. 5 shows examples of the two classes of filaments and their transforms).

The distribution of angular positions of subunits was determined as outlined in the Materials and Methods. The breadth of this distribution provides a measure of the disorder, reflecting the angular variation of the subunit from its ideal helical position. For pure actin, the value is ~12° (Stokes and DeRosier, 1987; Egelman et al., 1982). We found the angular disorder of the *Limulus* filaments to be ~4° and 3° for the 5.9 and 4.0 filaments, respectively. Stokes and DeRosier (1987), using an independent method for determining angular disorder, obtained a similar value (2°) for the 4.0 filaments. Thus, the amount of disorder is greatly reduced from that of pure actin. To assess whether the disorder was negligible for the purpose of 3D reconstruction, we calculated from it coherence lengths, which determine over what length the filament may be regarded as helical. If the length required for reconstruction is much less than this, the effect of angular disorder is essentially negligible. The coherence lengths are different for different layer lines used in the reconstruction (Egelman and DeRosier, 1982). With a disorder of 2°, the coherence length of the filament is at least 3,700 subunits for the sixth layer line and at least 233 subunits for the second layer line. Values intermediate between these apply to the remaining layer lines. This means that for the

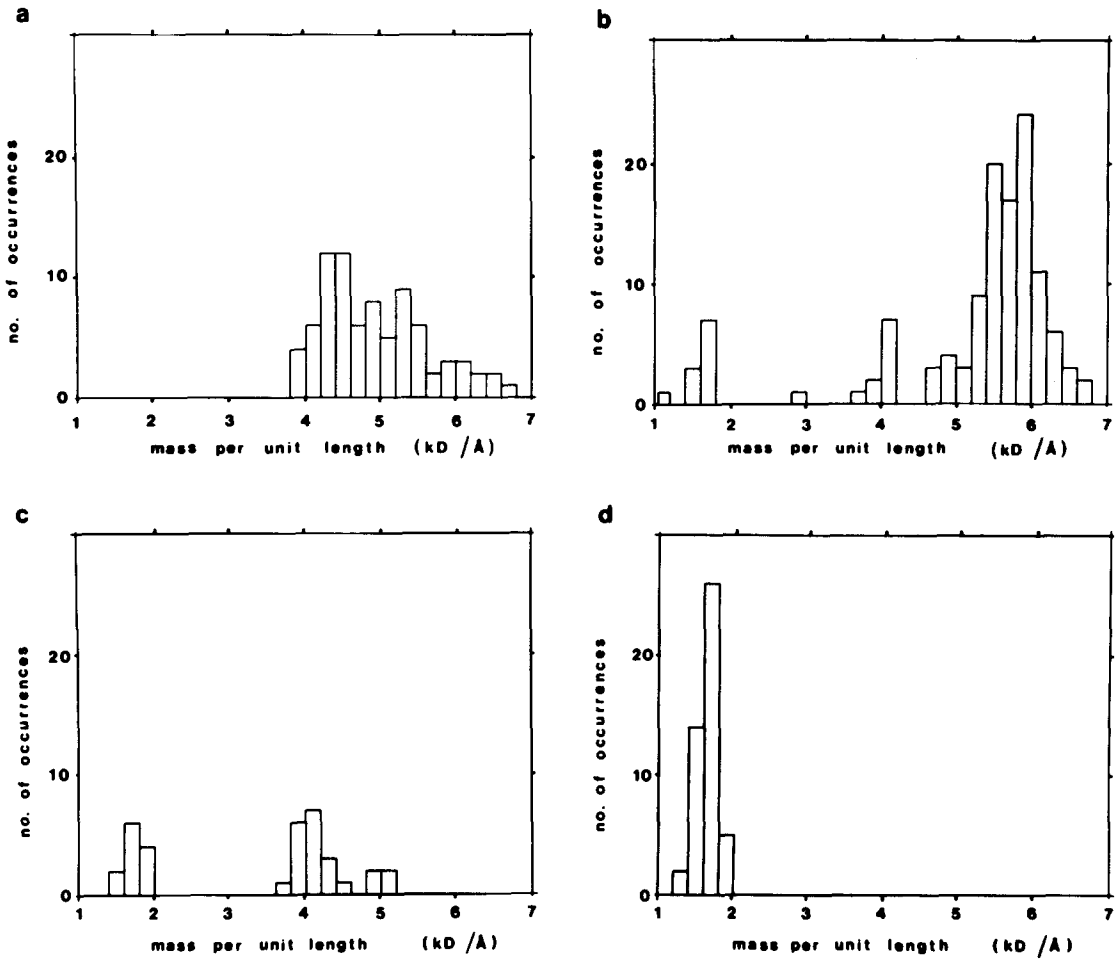

Figure 4. Histogram of the distribution of filaments according to their mass per unit length. (*a*) A preparation of filaments at an early stage of fraying. This preparation contained a mixture of filaments having mass/length of 4.0 and 5.9 kD/Å and of filaments with intermediate values. The filaments in this preparation were lying in patches of subunits, indicating their being caught during disassembly. (*b*) A preparation at a later stage than that in *a*. Images in which the background was free of unbound subunits were selected for measurement in order to obtain accurate values. This procedure also tends to eliminate filaments that are in the act of falling apart (as seen in *a*). Three discrete peaks, and hence three classes of filaments are seen: one at 1.6 kD/Å; one at 4.0 kD/Å; and one at 5.9 kD/Å. (*c*) A preparation at a later stage of disassembly. Only the lighter two classes of filaments are seen, corresponding to the peaks at 1.6 and 4.0 kD/Å. (*d*) A preparation of skeletal muscle F-actin treated with Triton X-100 and KSCN. A single peak at 1.6 kD/Å is seen.

length of the filaments we have used, 180 subunits or less, the filament may be assumed helical, and the 3D reconstruction can be carried out without the need for any correction.

3D Helical Reconstruction

Five *Limulus* 5.9 filaments and five 4.0 filaments were chosen for reconstruction based on their Fourier transforms (Fig. 5 shows an example of each type of filament and its corresponding Fourier transform). All these images were from negatively stained filaments examined by transmission electron microscopy, since freeze-dried STEM images showed only the first layer line and were therefore not suitable for helical reconstruction. As the first step of the reconstruction process, the helicity of the filaments was checked (as in DeRosier and Moore, 1970). The resulting values for the axial shift and tilt of the five 5.9 filaments and the five 4.0 filaments are shown in Table I. Values for Q of up to 30° are typical for negatively stained helical particles.

Next the filaments were aligned and scaled with respect to each other so the data could be averaged (Materials and Methods, Eq. 3; Amos, 1975). For the 5.9-filament data, this procedure was done for near and far side data separately, and then another iteration was performed to fit the average near and average far side data to each other. For the 4.0 filament data, this procedure was done for all data, and another iteration was performed fitting the data to the first average. The 35°-72° values we obtained for the minimum rms deviation of the correctly oriented filaments (Table II, second column) are typical for negatively stained helical particles; these values are always found to be higher than those found in simply locating the particle axis (Table I). We calculated three reconstructions, one from the average of the five 5.9 filament images, one from the five 4.0 filament images listed in Table I, and one from the three "best" 4.0 filament images, listed in Table II. These three 4.0 filaments were chosen because they had rms deviations of <50°. The two reconstructions of the 4.0 filaments (5 filaments vs. 3 filaments) did not differ significantly, but it seemed that morphological features were slightly better defined when only the three best images were

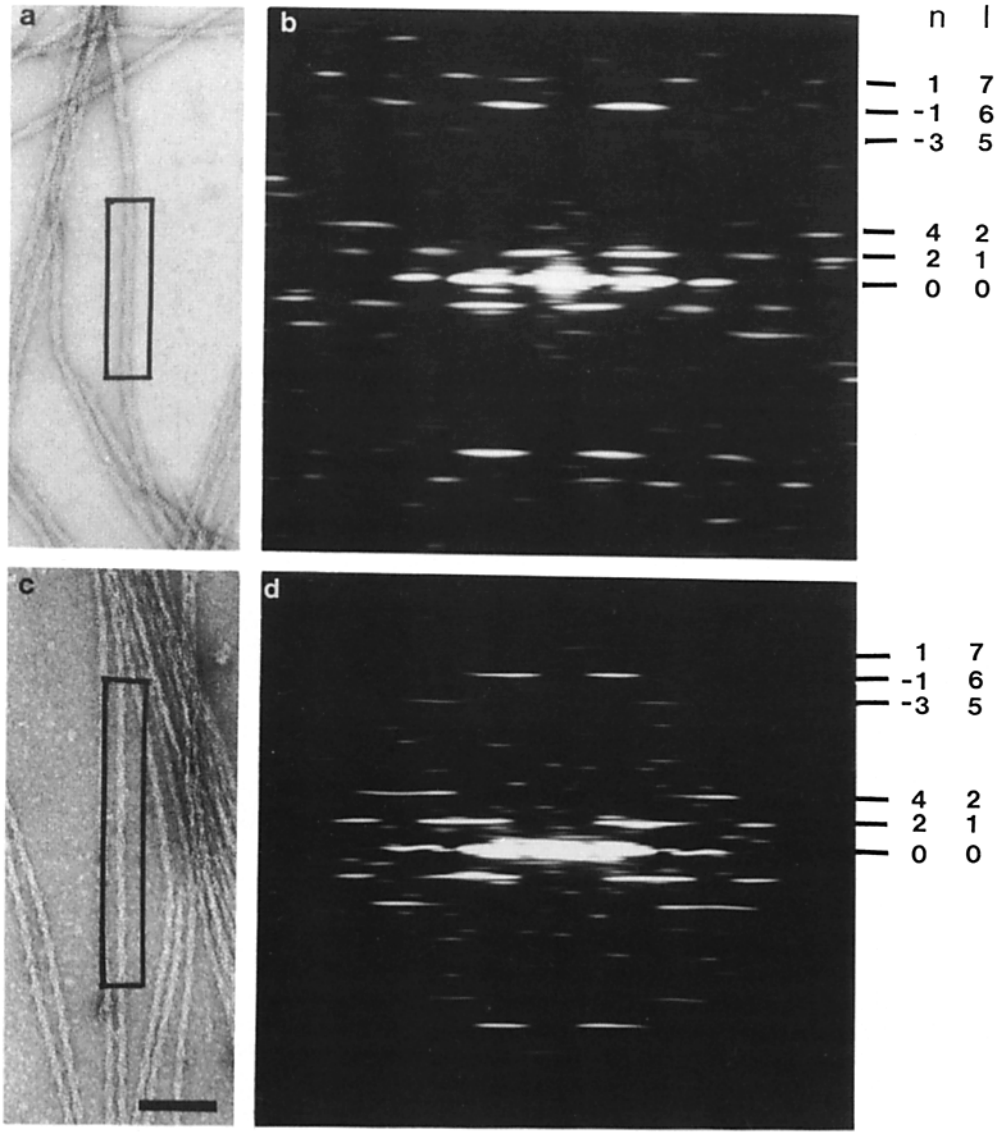

Figure 5. Electron micrographs of the 5.9- and 4.0-kD/Å filaments and their transforms. (*a*) A negatively stained 5.9-kD/Å filament. (*b*) Transform of filament in *a*. (*c*) A negatively stained 4.0-kD/Å filament. (*d*) Transform of filament in *c*. Bar, 1,000 Å.

Table I. Minimum Values of Q for Filaments Used in the 3D Reconstruction

Filament	Tilt angle	*y*-shift (pixels)	*Q*-min
4.0-a	0.0°	−1.5	7°
4.0-b	−2.5°	−1.0	12°
4.0-c	−2.8°	0.8	13°
4.0-d	2.0°	−0.5	77°
4.0-e	0.0°	0.0	22°
5.9-a	1.0°	−0.4	3°
5.9-b	−0.6°	1.2	23°
5.9-c	−1.6°	−0.6	5°
5.9-d	−0.4°	−0.3	4°
5.9-e	2.0°	−0.2	11°

Filaments preceded by 4.0- are of the 4.0 class; filaments preceded by 5.9- are of the 5.9 class. Shown for each filament are the tilt angle out of the plane of the micrograph and the *y*-shift from the center of the boxed image required to minimize *Q*, and the minimum value of *Q*.

used. The averaged Fourier coefficients, $G_{n,l}(R)$ and their transforms, $g_{n,l}(r)$ (Klug et al., 1958), are plotted in Fig. 6.

To determine the outer boundary of the reconstructions, we set the volume of the reconstruction to the expected volume. The expected value for the volume is obtained by dividing the molecular mass by 0.81 D/Å^3. For the 5.9 filament $V_{calculated}$ = 191,000 Å^3, and for the 4.0 filament $V_{calculated}$ = 131,000 Å^3. We contoured the 3D map, and for each contour determined the volume enclosed in the asymmetric unit. We then picked the contour corresponding to the expected value (Fig. 7).

The reliability of the reconstructions was examined by performing a Student's *t* test at the 99% confidence levels for each pixel in the reconstruction (Trachtenberg and DeRosier, 1987). Fig. 8 shows a section through each of the reconstructions together with *t* test maps. Fig. 9, *a* and *c* show surface representations of the 3D reconstructions of the 5.9 and 4.0 filaments, respectively.

Table II. Minimum Values of the Amplitude-weighted Phase Residuals for Filaments Used in the 3D Reconstructions

Filament	Phase residual -up-	Phase residual -down-	Degrees change up/down
4.0-a far	49°	77°	28
4.0-a near	38°	79°	41
4.0-b far	36°	71°	35
4.0-b near	36°	72°	36
4.0-c far	40°	71°	31
4.0-c near	35°	73°	38
5.9-a far	60°	83°	23
5.9-a near	71°	76°	5
5.9-b far	61°	75°	14
5.9-b near	55°	77°	22
5.9-c far	46°	80°	34
5.9-c near	50°	82°	32
5.9-d far	51°	72°	21
5.9-d near	72°	82°	10
5.9-e far	61°	79°	18
5.9-e near	46°	84°	38

Filaments preceded by 4.0- are of the 4.0 class; filaments preceded by 5.9- are of the 5.9 class. The minimum phase residuals, as computed by Eq. 3, are shown for each filament, including the minimum obtained when the filament is oriented incorrectly with respect to the average reconstruction for that class; that is, with its "barbed" end opposite that of the barbed end of the reconstructed filament. The "degrees change" between the "up" (correct) and "down" (incorrect) orientations gives an indication of the polarity of the filaments and the reliability of the choice of orientation.

Polarity of the 5.9 and 4.0 Filaments

It is now well known that actin filaments are polar. One way of establishing this polarity is to decorate the filaments with subfragment 1 (S1) of myosin (Huxley, 1963). Although the filaments in the *Limulus* acrosomal bundle do not decorate with S1, presumably because the 60- and 50-kD proteins inhibit binding, the polarity of the filaments in the *Limulus* bundle has been determined by assembling actin subunits on the ends of the bundle and then decorating the newly assembled ends (Tilney et al., 1981). They found that all actin filaments in the bundle have the same polarity and that the bundle tapers, with fewer filaments at one end than at the other. By simultaneously noting the bundle taper and the arrowheads on the decorated filaments at the ends of the bundle they showed that the thin end of the bundle is the "barbed" end of an S1 decorated actin filament. It would seem simplest to determine the orientation of frayed filaments relative to the taper of the bundle. This is not possible, however, because the fraying of the bundle, which is necessary to obtain individual filaments, obscures the taper.

To determine its polarity, the reconstruction of the 5.9 filaments (thought to be the filaments found in the intact *Limulus* bundle; see Discussion), was fit to images of intact bundles of known polarity as determined from their taper. To do the fitting, layer line data were sampled at row lines and fit to row line data from the transforms of four bundles using the amplitude-weighted phase residual shown in Eq. 3. A good fit was obtained for all four bundles, as shown in Table III. In subsequent figures we have placed the barbed end of the actin filaments, as determined from our reconstructions, at the top of the image.

Because it lacks the 50-kD subunit, the reconstruction of the 4.0 filaments could not be convincingly fit directly to the bundle as was done for the 5.9 filaments. To determine the orientation of the 4.0 filament in the bundle, we resorted to an indirect approach. We took a micrograph containing a segment of intact bundle with single 4.0 filaments fraying from its end (Fig. 2) and aligned the intact segment of bundle with respect to unfrayed bundles of obvious taper and hence of known polarity (Eq. 3, with no rotation permitted). This alignment procedure determined the polarity of the intact segment of the frayed bundle and also the polarity of the filaments fraying out from it. We then aligned the 3D reconstruction relative to the frayed, 4.0 filaments of now known orientation. Although the frayed filaments were not the best preserved filaments and were not those used in the reconstruction, they were good enough to determine the polarity of the reconstruction; phase residuals (Eq. 3) for the correct and incorrect filament orientations differed by 14°-27°.

As a check on the polarity determinations, we fit the reconstruction of the 5.9 filaments to the reconstruction of the 4.0 filaments, using the real-space residuals and checking both the up and the down orientations (for complete discussion see Materials and Methods). Because we could correct for the absence of the 50-kD subunit, this fitting led to a convincing result which agrees with that obtained directly; the real space residuals for the correct and incorrect orientations differed by 183%, whereas without the correction the difference was only 7%. All figures have their barbed, or "preferred," end at the top.

Location of the Auxiliary Proteins on the F-Actin Filaments

The 50-kD Protein. Having aligned the reconstruction of the 5.9 and 4.0 filaments as described previously, we subtracted the two to obtain a map of the 50-kD subunit (Figs. 7 *b*, 8, *e* and *f*, and 9 *b*). Before the subtraction the two reconstructions were scaled by minimizing the sum of the squared differences. The radial density profile ($g_{0,0}(r)$ of the Fourier transform) of the 5.9 minus the 4.0 reconstructions (that is, the 50-kD subunit) has its center of mass at 57 Å (Fig. 10 *d*, *dashed line*). A radial density profile (Stern et al., 1986) of the 50 kD subunit was also calculated from the STEM data by subtracting the radial density profile of the 4.0 filament from that of the 5.9 filament. The difference, which corresponds to the 50-kD subunit, has a peak at 53 Å (Fig. 10 *d*, *solid line*) in agreement with the previous result. Thus, results from the two independent methods agree.

60-kD Protein and Actin. We could not determine the position of the 60-kD subunit by subtracting an actin reconstruction from the reconstruction of the 4.0 filament since, due to angular disorder in F-actin, we had no reliable actin reconstruction. The reconstruction of the 4.0 filament, however, was very similar to the two-sphere model of F-actin proposed by Egelman and DeRosier (1983) but with a third morphological feature at larger radius, that is presumably the 60-kD protein (see *arrow*, Fig. 7 *c*). The diameters, moreover, were consistent with this interpretation: 91 Å for the actin "core" and 150 Å for the whole filament. That these filaments contain an F-actin core is supported by the observation that not only do they have the same helical symmetry as ac-

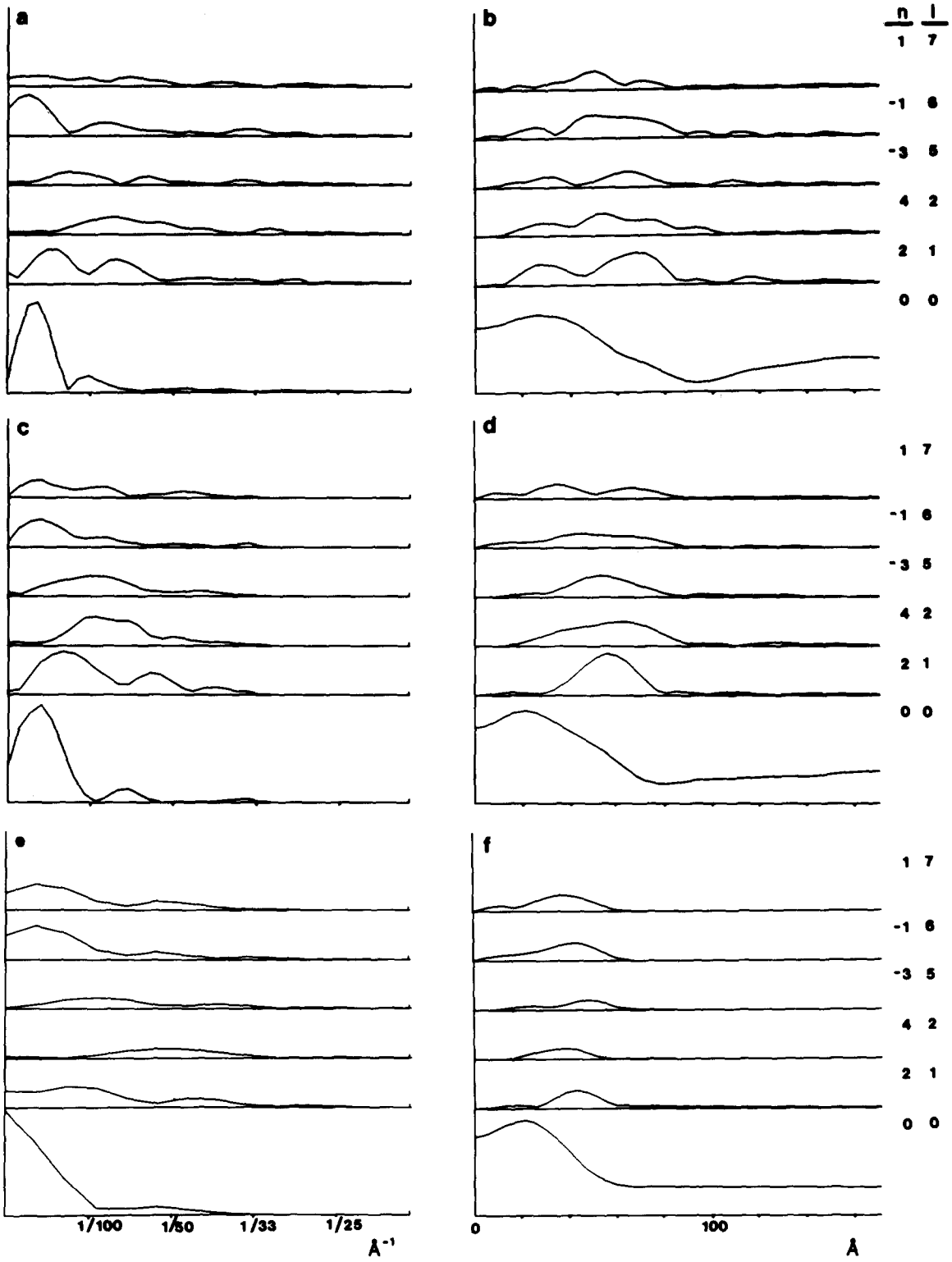

Figure 6. Layer line data for the 5.9 (*a* and *b*) and 4.0 (*c* and *d*) filaments, and for the actin filament derived from them (*e* and *f*). The left column shows the amplitudes of $G(n,l)(R)$ versus R, and the right column shows the amplitudes of $g(n,l)(r)$ versus r.

tin, but one can polymerize G-actin onto the end of the bundle (Tilney et al., 1981).

Difference profiles agree with this assignment of features to proteins: difference radial density profiles between the 4.0 filament reconstruction and the actin portion of the reconstruction of the 4.0 filament (see next paragraph) produced a peak at 49 Å corresponding to the 60-kD subunit (Fig. 10 *e*, *dashed line*). The position of the subunit was then determined, independently, from STEM data by subtracting the radial density profile of F-actin from the profile of the 4.0 filament (Fig. 10 *e*, *solid line*). The STEM result of 45 Å agrees with that obtained from the reconstruction.

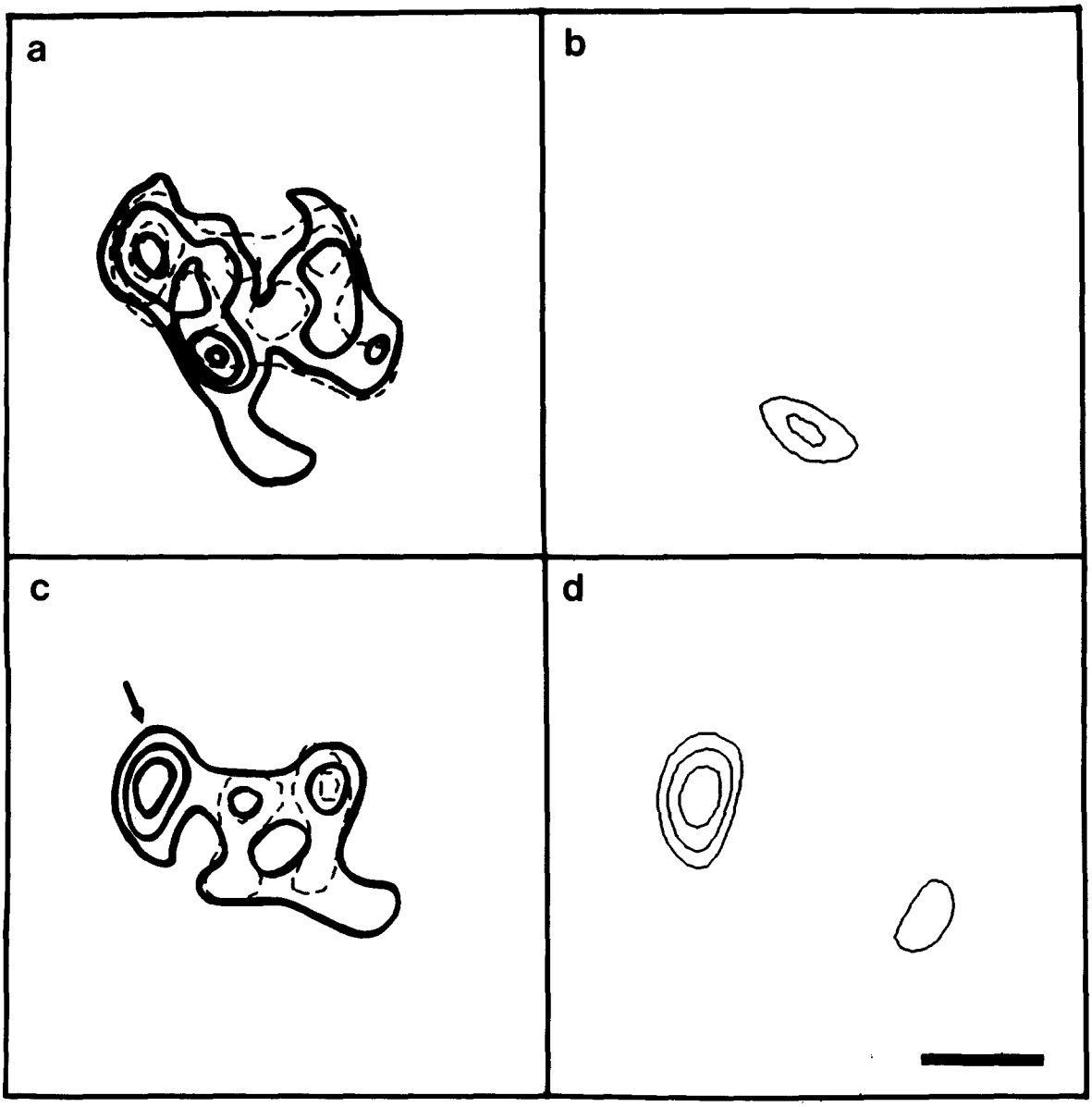

Figure 7. Transverse sections of the 5.9, 4.0, and 1.6 filaments, and the 50- and 60-kD subunits. (*a*) Superposed transverse section of the 5.9 (*solid line*) and 4.0 (*dashed line*) reconstructions. (*b*) Difference map obtained from the two maps shown in *a*; map corresponds to the 50-kD subunit. (*c*) Superposed transverse section of the 4.0 reconstruction (*solid line*) and the actin map (*dashed line*) derived from it. (*d*) Difference map obtained from the two maps shown in *c*; map corresponds to the 60-kD subunit. Bar, 50 Å.

To produce a map of the 60-kD subunit and of actin alone, we computationally removed the outermost morphological feature corresponding to the 60-kD protein from the 4.0 filament reconstruction. Fig. 7 *c* shows a cross section of the 4.0 filament reconstruction; there is a narrow "neck" in the upper left of the figure which appears to define the boundary between the actin and the outer 60-kD subunit.

After removing the outer feature, we smoothed the "cut" edges of the altered reconstruction by tapering the densities along the cut to zero to mimic the falloff at uncut edges of the filament. The data were further smoothed by computing a Fourier transform of the modified filament, filtering the transform by picking off only the data on layer lines l = 0, 1, 2, 5, 6, 7, and then recomputing the map.

The actin reconstruction so obtained (Figs. 7 *c*, *dashed line*, and 9 *c*) has a diameter of 91 Å. The actin subunit appears bilobed, with an outer lobe at 30 Å, and an inner lobe at 20 Å. These two lobes together form an actin subunit which is approximately perpendicular to the filament axis (see Discussion). The 60-kD subunit appears as an oblate spheroid (Figs. 7 *d* and 9 *d*).

Packing the 5.9 Filaments in a Bundle and Determining Interfilament Contacts

Copies of the 5.9 filament reconstruction were placed on an hexagonal lattice to produce a bundle, and projections of the bundle were compared with electron micrographs of actual bundles (Fig. 11). The filaments in the micrographs of bundles chosen for comparison are all in register, so the cross-

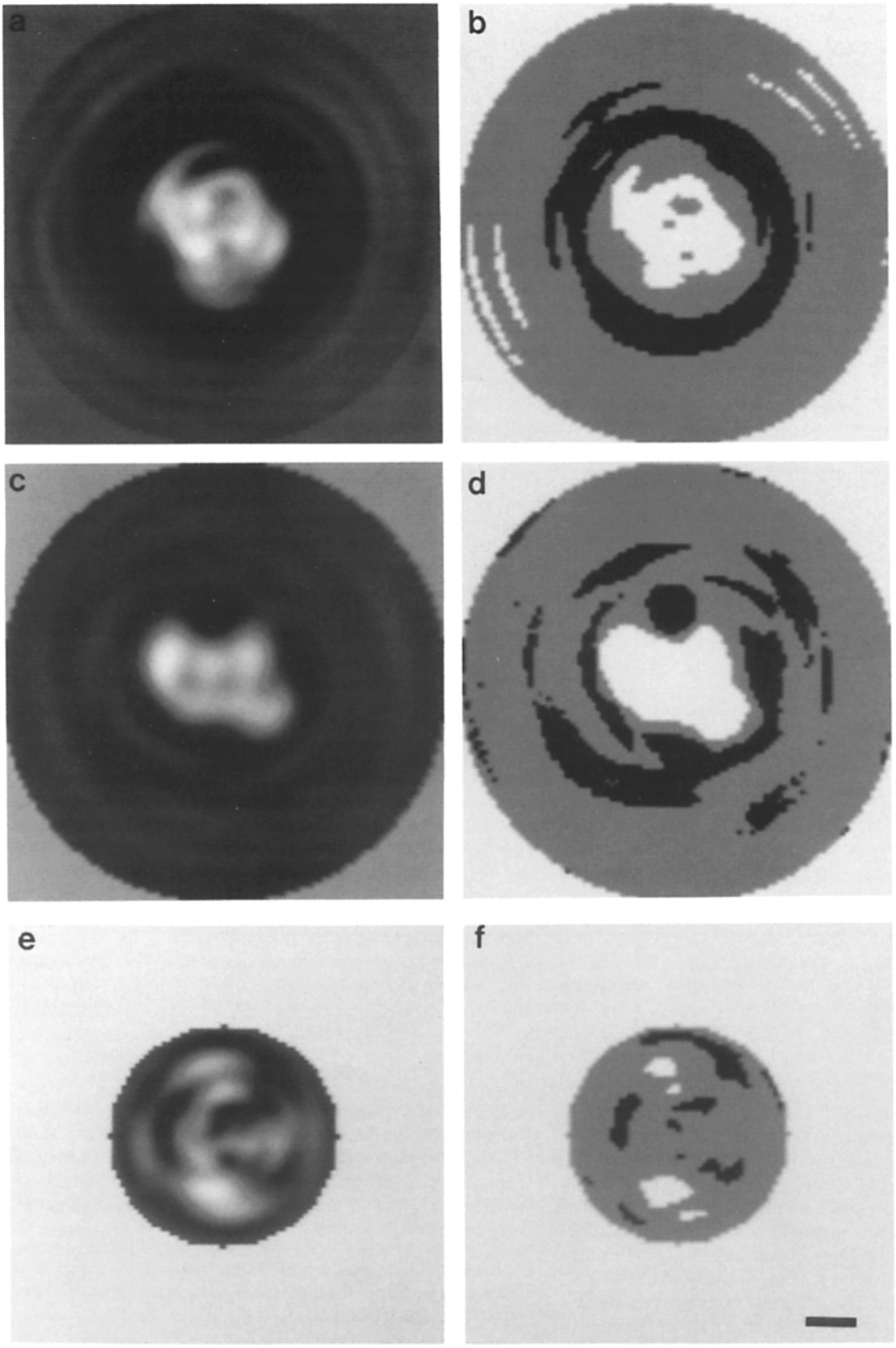

Figure 8. Sections of the 3D maps (left column) and the corresponding *t* test maps (right column). The left column of panels shows in a grey scale representation the density for a section taken perpendicular to the helix axis. Each pixel represents the average of several independent measurements derived from the set of contributing images. Alongside it is a *t* test map, which assesses the significance of these averaged densities. Three levels are displayed: white for densities that are significantly positive at the 99% confidence level, black for those significantly negative, and grey for values not significantly different from zero. (*a* and *b*) 5.9 filaments. (*c* and *d*) 4.0 filaments. (*e* and *f*) Difference map of 5.9 and 4.0 filaments and *t* test map of the difference. Bar, 50 Å.

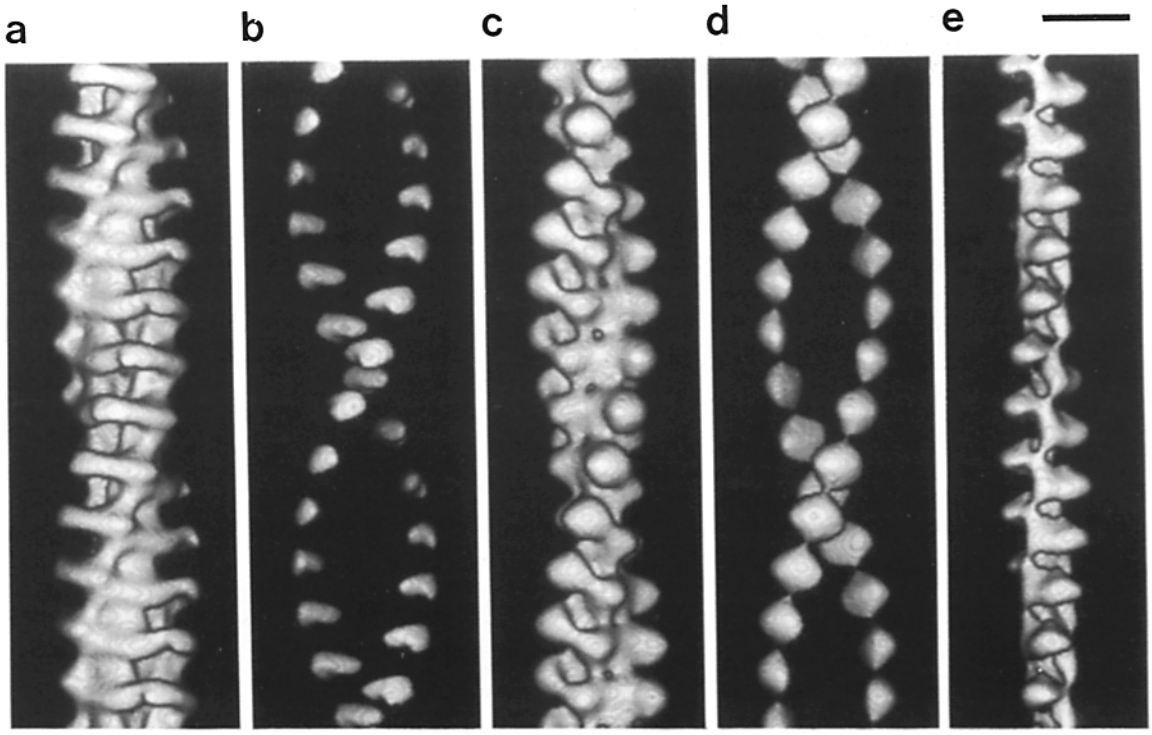

Figure 9. Surface views of the filaments and subunits. (*a*) 5.9 filament. (*b*) 50-kD subunit. (*c*) 4.0 filament. (*d*) 60-kD subunit. (*e*) Actin filament. Bar, 100 Å.

over of one filament is at the same axial position as those of its neighbors (Tilney, 1975). The interfilament spacing of filaments which give the best fit to actual micrographs is 130 Å.

To examine the packing contacts between filaments in a bundle we produced bundles from the difference maps showing just the auxiliary proteins, in addition to a bundle of the reconstructed 5.9 filaments. Fig. 12 *a* shows a two-filament bundle of the 5.9 filaments side by side. Fig. 12 *b* shows a two-filament bundle in which only the 60-kD subunit is visible. Similarly, Fig. 12 *c* shows one filament with the 60-kD subunit visible and one filament with the 50-kD subunit visible, and Fig. 11 *d* shows a two-filament bundle in which only the 50-kD subunit is visible. There appear to be extended contacts between the 60-kD proteins of adjacent filaments, but there may also be 50–50-kD and/or 50–60-kD protein contacts (see Discussion).

Table III. Minimum Values of the Amplitude-weighted Phase Residuals for Bundles Used to Determine the Polarity of the 3D Reconstructions

Bundle	Phase residual -up-	Phase residual -down-	Degrees change up/down
B-1far d=105	32°	58°	16
B-1near	44°	56°	12
B-2far d=130	35°	48°	13
B-2near	23°	54°	31
B-3far d=130	39°	58°	19
B-3near	39°	59°	20
B-4far d=105	38°	52°	14
B-4near	31°	58°	27

The minimum phase residuals were computed by using Eq. 3 with no rotation permitted ($\Delta\phi = 0$). The bundle data were sampled at row lines corresponding to *d*, the interfilament spacing, as were the 3D reconstruction data. The minimum phase residuals are shown for each bundle, including the minimum obtained when the bundle is oriented incorrectly with respect to the 3D reconstruction; that is, with its "barbed" end opposite that of the barbed end of the reconstructed filament. The "degrees change" between the "up" (correct) and "down" (incorrect) orientations gives an indication of the polarity of the filaments and the reliability of the choice of orientation.

Discussion

Bundle and Filament Composition

Three classes of filaments (that is, 1.6, 4.0, and 5.9 kD/Å) are found in preparations of frayed bundles by STEM. The STEM measurements together with 3D reconstructions suggest these classes are actin, actin plus a 60-kD subunit, and actin plus a 60-kD subunit and a 50-kD subunit, respectively. Simulations of the bundle produced from 3D reconstruction of the 5.9 filaments reproduce very accurately the details seen in electron micrographs of the intact bundle (Fig. 11). The uniformity of the filaments seen in transverse and longitudinal sections of the bundle (see Tilney, 1975) are consistent with there being only one type of filament, which we therefore suggest is the 5.9 filament.

SDS-PAGE of the bundle, therefore, should show equimolar amounts of actin, the 50-, and the 60-kD proteins. There are indeed three bands at approximately the correct molecular masses. The band at ~60 kD, however, appears considerably less dense than those of the actin and 50-kD protein. The explanation of the weakness of this band is not clear. It may be that the bundle contains more than one class of filament, although we think this unlikely in view of the results from electron microscopy. Alternatively, it may be that the

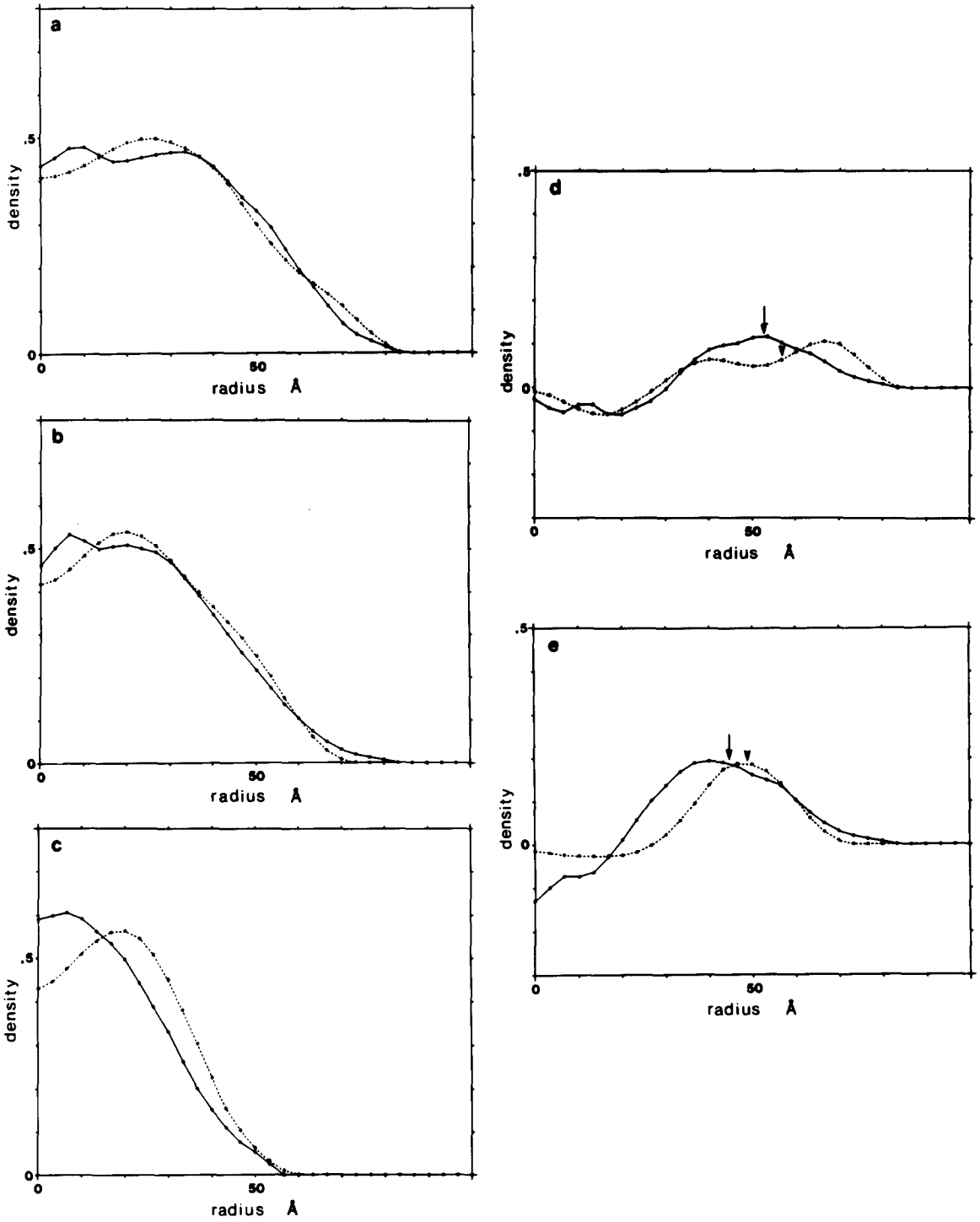

Figure 10. Radial density profiles from STEM (*solid lines*) and 3D reconstructions of electron micrographs (*dashed lines*). Relative scaling was done by least squares minimization of the differences. Arrows indicate the centers of mass for the auxiliary proteins as located by STEM. Arrowheads indicate the centers of mass for the auxiliary proteins as located by 3D reconstruction. (*a*) 5.9 filaments. (*b*) 4.0 filaments. (*c*) Skeletal muscle F-actin (STEM) and actin portion of the 4.0 filament map. (*d*) 50-kD subunit (*a* minus *b*). (*e*) 60-kD subunit (*b* minus *c*).

60-kD protein is not as intensely stained as the other two or it may be that the preparation is contaminated.

Assignment of Morphological Features to Proteins

We assigned the outermost, armlike feature of the 5.9 filament reconstruction to the 50-kD protein. This assignment was made from a straightforward difference map of the 5.9 minus the 4.0 reconstructions. From our STEM data, the difference in these two filaments is the 50-kD protein present on the 5.9 but not the 4.0 filament. We assume that the binding of the 50-kD protein produces no significant morphological changes in the actin or 60-kD protein at the resolution

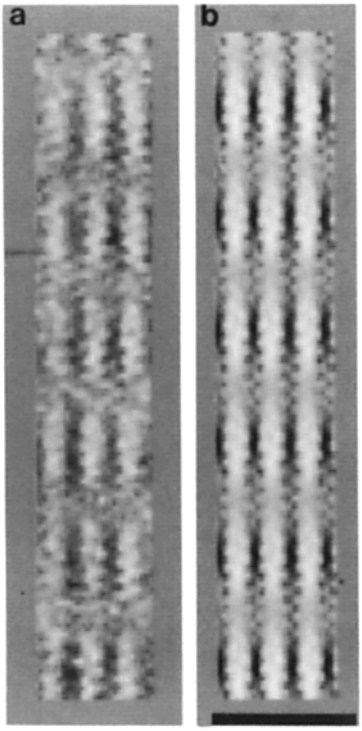

Figure 11. Comparison of an electron micrograph of a bundle with a simulated bundle. (*a*) Electron micrograph of a negatively stained, intact bundle. (*b*) Projection of a bundle generated by arranging reconstructions of the 5.9 filaments on an hexagonal lattice. Bar, 500 Å.

of our data. The appearance of a single, well-defined peak in the difference map (Fig. 7 *b*) reinforces this interpretation. The radial density of the difference data, $g_{0,0}(r)$, locates the 50-kD protein at 57 Å (Fig. 10 *d*, *dashed line*). Consistent with the above interpretation is that radial density profiles from STEM data of the 5.9 minus the 4.0 filaments locate the extra mass (50 kD) at about the same radius, 53 Å (Fig. 10 *d*, *solid line*). Although the peaks of the two difference profiles are at about the same position, the profiles are not identical. This is also true for the profiles corresponding to the 60-kD subunit. Which profile is more faithful is not known. On the one hand, equatorial data corresponding to the negatively stained filaments do not faithfully represent the radial density profile of the structure because the shell of negative stain is not cylindrically symmetric. On the other hand, the freeze-dried preparations of the STEM do not preserve the subunit detail and therefore may not preserve the radial density profile.

We assigned the outermost density of the 4.0 filament reconstruction to the 60-kD protein. This assignment was based on the assumption that the radial position of the outermost density from negatively stained preparations, 49 Å, is too far from the helical axis to be actin. In addition, differences between STEM radial density profiles for 4.0 filaments minus actin have a peak whose center of mass is at 45 Å, supporting this assignment (Fig. 10 *e*).

Actin Portion of the Limulus Filament

The actin filament, which we carved out of the *Limulus* 4.0 reconstruction, has a diameter of 91 Å (Figs. 7 and 9), in agreement with the 90–100 Å found by Amos et al. (1982), O'Brien et al. (1983), Egelman and DeRosier (1983), and others (see reviews by Amos, 1985 and Egelman, 1985). This map of actin is strikingly similar in appearance to the reconstruction of frozen-hydrated actin filaments done by Trinick et al. (1986).

The actin monomer in our actin map consists of two lobes, with the long axis of the monomer (that is, the line between the centers of the two lobes) at an angle of ~90° relative to

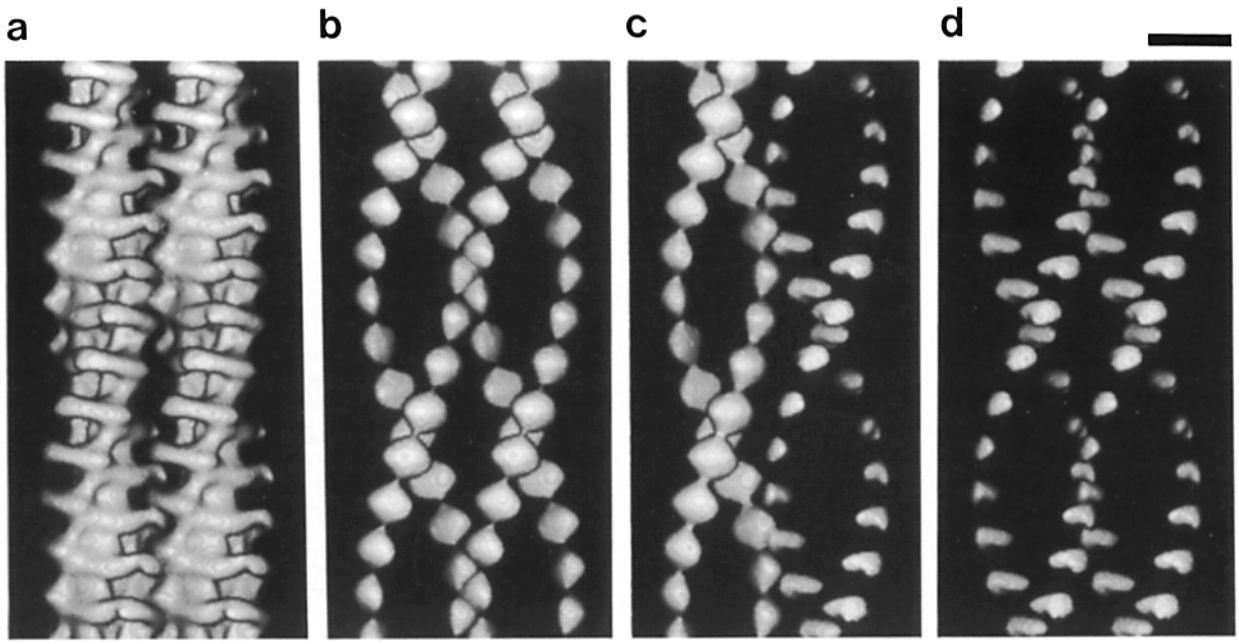

Figure 12. Packing contacts in the bundle. (*a*) Two 5.9 filaments arranged as in a bundle at a separation of 130 Å. (*b*) The same filaments but with the actin and 50-kD subunits not shown; the 60-kD subunits are seen. (*c*) The same filaments but with the left showing only the 60-kD subunits and the right showing only the 50-kD subunits. (*d*) The same filaments but with the actin and 60-kD subunits not shown; the 50-kD subunits are seen. Bar, 100 Å.

the filament axis (Fig. 9 *e*). The choice of which pair of inner lobe and outer lobe constitute a monomer was based on the choice made by Egelman and DeRosier (1983). The dimensions of the actin subunit are ~70 × 40 × 35 Å (cf. dimensions of 67 × 40 × 37 Å for the Suck et al. [1981] actin subunit and 70 × 40 × 38 Å for the Sakabe et al. [1983] actin subunit seen in crystals of actin + DNase I). To measure the sizes of the two lobes we divided the monomer perpendicular to its long axis at a point where there is an indentation in its surface. The outer lobe is spheroidal, has a diameter of 35 Å, and lies with its center at 30 Å. The inner lobe is a prolate ellipsoid with its long axis nearly parallel to the filament axis. This inner lobe has dimensions of 48 × 25 × 25 Å and its center at 20 Å from the helix axis (Fig. 9 *e*).

Connectivity within the actin filament occurs between actin monomers along the one-start and the two-start helices. The outer lobe of the actin subunit has contacts only to the nearest actin monomer along the one-start; this connection is between the outer lobe of one actin subunit and the inner lobe of the adjacent subunit (Fig. 9 *e*). The weak connection along the two-start is between inner lobes of the actin subunits. This weak connectivity along the two-start contrasts with a very strong connectivity in the actin reconstruction of Aebi et al. (1986) and with no connectivity in the reconstruction of Trinick et al. (1986). The connectivity in our map may be real or may be an artifact due to the limited axial resolution, to stain withdrawal during exposure to the electron beam, or to errors in the excision of the 60-kD subunit.

Shape and Actin-binding Contacts of Auxiliary Proteins

The 60-kD protein is shaped like a teardrop, and has dimensions of 54 × 54 × 40 Å. The 60-kD protein has its most extensive contact with the inner lobe of actin, with a smaller contact at the outer lobe of the same actin monomer (Figs. 7 *c* and 9, *d* and *e*). The 50-kD protein is arm shaped, linking the protein on one of actin's twin strands to the outer lobe of the actin subunit on the opposite strand (see Fig. 9, *a* and *b*). The 50-kD protein has two portions, one 22 × 50 × 28 Å and one 31 × 40 × 34 Å connected by an elbow bend of 160°.

Packing Contacts in the Limulus Bundle

In Fig. 12, which shows the 3D reconstruction of two filaments side by side as in a bundle, the largest areas of contact are seen to be between pairs of 60-kD proteins on adjacent filaments, with less extensive contacts between adjacent 60- and 50-kD subunits. There are two functional properties of the bundle which it is tempting to ascribe to the 50- and 60-kD subunits. The first is the crossbridging of filaments and the second is the change in twist that drives extension of the bundle (DeRosier et al., 1982).

The interactions of the protein subunits suggest the role of each subunit. The 60-kD protein has its main contacts with the inner lobe of an actin subunit on one filament and a 60-kD subunit on an adjacent filament. Our speculation is that this is the bundling protein. The 50-kD protein, however, has its main contacts between the outer lobe of an actin subunit and the 60-kD subunit on the other strand of the same filaments. Thus it spans the two strands of the actin filament. Our speculation is that the 50-kD protein plays a role in the change of twist of the filaments.

We thank Peter Vibert for innumerable discussions and assistance, and Noreen Francis for biochemical assistance. We thank Paul Matsudaira for his SDS-PAGE results, and the Brookhaven National Lab staff for their assistance and computer programs. We thank David Stokes for editorial comments, and Judy Black for photography.

This work was supported by National Institutes of Health (NIH) grant GM 26357 (E. S. A. Bullitt and D. J. DeRosier), NIH training grant 2T32GM07596-6 (E. S. A. Bullitt), NIH grant HD14474 (L. G. Tilney), and Muscular Dystrophy Association postdoctoral fellowship (L. M. Coluccio).

Received for publication 10 February 1988, and in revised form 11 April 1988.

References

Aebi, U., R. Millonig, H. Salvo, and A. Engel. 1986. The three-dimensional structure of the actin filament revisited. *Ann. NY Acad. of Sci.* 483:100–119.

Amos, L. A. 1975. Combination of data from helical particles: correlation and selection. *J. Mol. Biol.* 99:65–73.

Amos, L. A. 1985. Structure of muscle filaments studied by electron microscopy. *Annu. Rev. Biophys. Biophys. Chem.* 14:291–313.

Amos, L. A., H. E. Huxley, K. C. Holmes, R. S. Goody, and K. A. Taylor. 1982. Structural evidence that myosin heads may interact with two sites on F-actin. *Nature (Lond.).* 299:467–469.

DeRosier, D. J., and R. Censullo. 1981. Structure of F-actin needles from extracts of sea urchin oocytes. *J. Mol. Biol.* 146:77–99.

DeRosier, D. J., and P. B. Moore. 1970. Reconstruction of three-dimensional images from electron micrographs of structures with helical symmetry. *J. Mol. Biol.* 52:355–369.

DeRosier, D. J., E. Mandelkow, A. Silliman, L. Tilney, and R. Kane. 1977. Structure of actin-containing filaments from two types of non-muscle cells. *J. Mol. Biol.* 113:679–695.

DeRosier, D. J., L. G. Tilney, E. Bonder, and P. Frankl. 1982. A change in twist of actin provides the force for the extension of the acrosomal process in *Limulus* sperm: the false-discharge reaction. *J. Cell Biol.* 93:324–337.

DeRosier, D., L. Tilney, and P. Flicker. 1980. A change in the twist of the actin-containing filaments occurs during the extension of the acrosomal process in *Limulus* sperm. *J. Mol. Biol.* 137:375–389.

Egelman, E. H. 1985. The structure of F-actin. *J. Muscle Res. Cell Motil.* 6:129–151.

Egelman, E. H., and D. J. DeRosier. 1982. The Fourier transform of actin and other helical systems with cumulative angular disorder. *Acta Crystallogr. Sect. B Struct. Crystallogr. Cryst. Chem.* A38:796–799.

Egelman, E. H., and D. J. DeRosier. 1983. A model for F-actin derived from image analysis of isolated filaments. *J. Mol. Biol.* 166:623–629.

Egelman, E. H., N. Francis, and D. J. DeRosier. 1982. F-actin is a helix with a random variable twist. *Nature (Lond.).* 298:131–135.

Huxley, H. E. 1963. Electron microscope studies on the structure of natural and synthetic protein filaments from striated muscle. *J. Mol. Biol.* 7:281–308.

Klug, A., F. H. C. Crick, and H. W. Wyckoff. 1958. Diffraction by helical structures. *Acta Crystallogr.* 11:199–213.

Laemmli, U. K. 1970. Cleavage of structural proteins during the assembly of the head of bacteriophage T4. *Nature (Lond.).* 227:680–685.

O'Brien, E. J., J. Couch, G. R. P. Johnson, and E. P. Morris. 1983. *In* Actin: Its Structure and Function in Muscle and Non-Muscle Cells. C. Dos Remedios and J. Barden, editors. Academic Press, Inc., New York/London. 3–16.

Sakabe, N., K. Sakabe, K. Sasaki, H. Kondo, T. Ema, N. Kamiya, and M. Matsushima. 1983. Crystallographic studies of the chicken gizzard G-actin·DNaseI complex at 5-Å resolution. *J. Biochem.* 93:299–302.

Spudich, J. A., and S. Watt. 1971. The regulation of rabbit skeletal muscle contraction. *J. Biol. Chem.* 246:4866–4871.

Steven, A. C., J. F. Hainfeld, B. L. Trus, P. M. Steinert, and J. S. Wall. 1984. Radial distributions of density within macromolecular complexes determined from dark-field electron micrographs. *Proc. Natl. Acad. Sci. USA.* 81:6363–6367.

Steven, A. C., T. A. Simpson, B. L. Trus, P. S. Furcinitti, J. F. Hainfeld, and J. S. Wall. 1986. Radial density profiles of macromolecular filaments determined from dark-field scanning transmission electron micrographs. *Ann. NY Acad. Sci.* 483:188–198.

Stokes, D. L., and D. J. DeRosier. 1987. The variable twist of actin and its modulation by actin-binding proteins. *J. Cell Biol.* 104:1005–1017.

Suck, D., W. Kabsch, and H. G. Mannherz. 1981. Three-dimensional structure of the complex of skeletal muscle actin and bovine pancreatic DNase I at 6-Å

resolution. *Proc. Natl. Acad. Sci. USA.* 78:4319–4323.
Tilney, L. G. 1975. Actin filaments in the acrosomal reaction of *Limulus* sperm. *J. Cell Biol.* 64:289–310.
Tilney, L. G., E. M. Bonder, and D. J. DeRosier. 1981. Actin filaments elongate from their membrane-associated ends. *J. Cell Biol.* 90:485–494.
Trachtenberg, S., and D. J. DeRosier. 1987. Three-dimensional structure of the frozen-hydrated flagellar filament. The left-handed filament of *Salmonella typhimurium*. *J. Mol. Biol.* 195:581–601.
Trinick, J., J. Cooper, J. Seymour, and E. H. Egelman. 1986. Cryo-electron microscopy and three-dimensional reconstruction of actin filaments. *J. Microsc. (Oxf.).* 141:349–360.
Wall, J. S., and J. F. Hainfeld. 1986. Mass mapping with the scanning transmission electron microscope. *Annu. Rev. Biophys. Biophys. Chem.* 15:355–376.